

Nuclear Neutron Haloes as Seen by Antiprotons

S. Wycech* and R. Smolańczuk†

Sołtan Institute for Nuclear Studies,
Hoża 69, PL-00-681 Warsaw, Poland

Abstract

Nuclear interactions of antiprotons in atomic states are discussed. The total as well as partial widths for single nucleon capture events are calculated. These are compared to the X-ray and recent single nucleon capture data. The rates of the neutron or proton captures test nuclear density distributions at the extreme nuclear surface. Recently found cases of neutron and proton haloes are analysed.

1 Introduction

It has been known for a long time that hadronic atoms are a way to test the nuclear surface region: the tail of nuclear density distribution, its isospin structure and correlations [1]. There are two methods to learn these properties:

1) *Measurements of the X ray cascade in hadronic atoms that provide atomic levels and widths.* Some fractions of the level energies are due to nuclear interactions and some parts of the widths are due to nuclear captures of the hadron. For highly excited atomic states the nuclear effects are small, for low levels the nuclear capture probability increases rapidly with decreasing orbital radii and the cascade terminates suddenly. These natural limitations allow to measure one level width per atom. Only in some special cases two widths and one level shift may be obtained. The levels in question are of large angular momenta that locate the nuclear interactions on the nuclear surface. At first, the atomic data are used to learn the strength and form of hadron optical potentials. Next, some of the level widths may be used to test the nuclear density tail. The shifts are usually difficult to interpret and provide a check on the optical potential.

2) *Measurements of the nuclear capture products.* A unique determination of the emitted particles may discriminate captures on protons from captures on neutrons and signal nuclear correlations. Many experiments using various

*Internet address: wycech@fuw.edu.pl

†Internet address: smolan@fuw.edu.pl

detection techniques have presented data, in principle, more informative than the X-ray data. Unfortunately, these are also more difficult to interpret as the initial atomic states are not known and the final state interactions, in particular the charge exchange reactions, are uncertain.

Some related results in the \bar{p} and other atoms are discussed in reviews [2,9] and other talks at this meeting. This paper discusses the neutron density distributions tested by recent antiprotonic CERN experiments, [3]. The latter are of the second kind and follow previous antiprotonic [4] and kaonic [5] studies. Now, however, the separation of $\bar{p}p$ and $\bar{p}n$ annihilation modes is done in a different way. Instead of the final state mesons it is the final nucleus that is detected by radiochemical methods. In this way the rates of reactions $\bar{p}(N, Z) \rightarrow \text{mesons}(N - 1, Z)$ and $\bar{p}(N, Z) \rightarrow \text{mesons}(N, Z - 1)$ are found. The ratio of these rates allow to detect the number of neutrons relative to the number of protons in the region of nuclei where the \bar{p} capture occurs. The measurements done in nuclei where the method is applicable yield results that differ widely. For some nuclei ($^{58}\text{Ni}, ^{96}\text{Ru}$) one finds the n/p ratio about unity, in heavy nuclei ($^{176}\text{Yb}, ^{232}\text{Th}, ^{238}\text{U}$) it is as large as 5 or 8 while in ^{144}Sm it happens to be significantly less than unity. Once the final and initial states are known and the reaction mechanism is understood one can determine where the capture occurs and what nuclear region is tested by these experiments. Then one can interpret the n/p ratio in terms of "neutron halo" or "neutron skin" and give more precise meaning to these terms. The purpose of this work is the presentation of the basic elements of such an analysis [6].

The known difficulties: uncertainty of the capture state and the necessity to describe the final state interactions are still present. In particular, the radiochemistry is selective, only cold final nuclei are seen and a proper description of the final states becomes a question. Fortunately an additional constraint follows from the measurement itself. It is given by the ratio of two capture rates: the rate for single nucleon captures that end with cold residual nuclei and the total capture rate. The former, cold captures, amount to 10-20 percent of the total, and are almost independent on the nucleus. If the capture occurs from a definite atomic state the total rate is given by the level width and is in principle measurable by the X-rays. Such clean experiments are not feasible, yet. The chances of nuclear capture from various initial \bar{p} states have to be calculated with an optical potential derived from other atomic data. An experimental check is expected with forthcoming CERN experiments which hopefully will supply also the transition probabilities per single stopped antiproton [6].

Next sections describe briefly: the optical potential, final state mesonic interactions and the interpretation of the neutron haloes.

2 Nuclear Interactions of Atomic Antiprotons

Antiprotons captured into atomic orbits cascade down, emitting Auger electrons and X-rays, to be finally absorbed by the nucleus. This happens in atomic states of high angular momenta, presumably in circular orbits. Such a scenario is formed by the atomic cascade that tends to populate states of high angular momenta l . Because of the centrifugal barriers and large $N\bar{N}$ absorptive cross sections, the nuclear interaction of \bar{p} is rather well localised at distances as large as twice the nuclear radius. An important aspect of such peripherality is that it allows low density approximations in the theoretical description: quasi-free interactions and a single particle picture of the nucleus. It also facilitates the description of final mesons, an important issue in understanding of the absorption experiments. On the other hand, the surface studies are complicated by the sensitivity of results to an uncertain range of hadron-nucleon forces.

Here, we present a phenomenological description of the antiproton absorption by nuclei. The level widths are calculated in terms of \bar{p} optical potentials. The simplest one, linear in nuclear density, is of the form [7]

$$V^{\text{opt}}(\vec{R}) = \frac{2\pi}{\mu_{N\bar{N}}} t_{N\bar{N}} \rho(\vec{R}) \quad (1)$$

where $\mu_{N\bar{N}}$ is the reduced mass, $\rho(\vec{R})$ is a nuclear density and $t_{N\bar{N}}$ is a complex scattering length. The density $\rho(\vec{R})$ in Eq.(1) is not the "bare" nucleon density $\rho_0(\vec{R})$ but a folded one

$$\rho(\vec{R}) = \int d\vec{u} \rho_0(\vec{R} - \vec{u}) v(\vec{u}) \quad (2)$$

where v is a formfactor that describes the $N\bar{N}$ force range. The length $t_{N\bar{N}}$ in Eq.(1) is extracted from the most precise X-ray measurements done in oxygen isotopes, [7]. The best fit to these data yields $t_{N\bar{N}}$ of about $-1.5 - i2.5$ fm, [7,8]. The corresponding potential is deep and black. For the central densities, $\Im V^{\text{opt}}$ is 200 MeV strong and the mean free path is well below 1 fm. However, both the form and the strength of V^{opt} are tested only in the surface region. Thus, $\Im V^{\text{opt}}$ is determined by the atomic level widths, given by

$$\Gamma = 4 \frac{\pi}{\mu_{N\bar{N}}} \Im t_{N\bar{N}} \int d\vec{R} \rho(\vec{R}) |\Psi_{\bar{N}}(\vec{R})|^2 \quad (3)$$

where $\Psi_{\bar{N}}(\vec{R})$ is the atomic wave function. Since $\Psi_{\bar{N}} \approx R^l$ is determined essentially by the angular momentum l and only high momentum states are available the absorption strength is peaked at the surface.

A typical nuclear interaction region in ^{58}Ni is shown in Fig.1, where the absorption density $W = \rho |\Psi|^2 R^2$ is plotted. There are two special atomic states in the capture process. One is called an "upper" level which usually is

the last one that can be detected by the X rays before the cascading down \bar{p} is absorbed. Its width is obtained from the intensity loss of X-ray transitions. In this and in many other nuclei the absorption is most likely to happen from this level. The next circular state below it, "the lower state", may be reached in some nuclei. In such a case one measures the shape of X-ray line and extracts the level width and shift. Nuclear absorptions may happen also in higher atomic orbits in a way that is not detected by X-ray studies. The chances for the \bar{p} to reach the low levels in question are not known well.

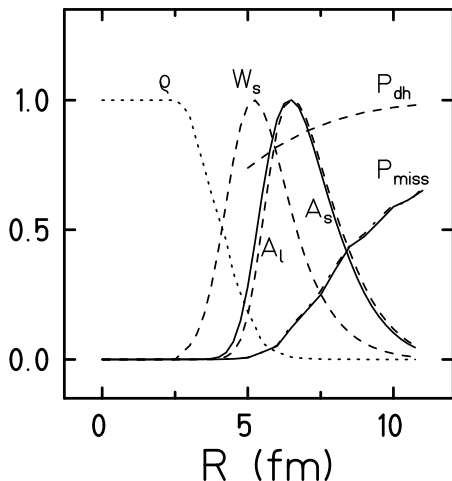


Figure 1: The antiproton absorption densities from $n=6, l=5$ (upper level) in ^{58}Ni : W_s for the $N\bar{N}$ annihilation range $r_o = .75$ fm, ρ is a "bare" neutron density. The cold antiproton absorption densities on a neutron (integrand in Eq.(4)): A_l for the $N\bar{N}$ annihilation range $r_o = 1$ fm and A_s for the range $r_o = .75$ fm. Normalisations are arbitrary. Missing probabilities (left scale): P_{miss} continuous is due to phase space alone, P_{miss} dash-dotted is calculated with corrections for the experimental pion momentum distribution. The flat dashed curve is P_{dh} from the HF model.

The peripherality of capture depends on the range of $N\bar{N}$ forces. The range parameters in Eq.(2) may be adjusted to fit the atomic and low energy scattering data. Gaussian profile formfactors $\exp(-(r/r_o)^2)$ have been used, [8], and typical best fit values are: $r_{oi} \approx 1$ fm (for $\Im V$) and $r_{or} \approx 1.5$ fm (for $\Re V$). On the other hand, calculations based on the $N\bar{N}$ potentials yield values r_{oi} of 0.7 fm up to 1.5 fm, [11], for different $N\bar{N}$ states and different ways to go off-shell. The latter values are probably the upper and lower limits of r_{oi} , while the best fit number is located in-between. An effect of the range uncertainty is shown in Fig.1 for a partial decay width. The effect on the full width is essentially the

same.

Optical model calculations based on the $N\bar{N}$ interaction potentials [10,11] show that the lengths $t_{N\bar{N}}$ are not the $N\bar{N}$ S-wave scattering lengths. The latter are smaller and repulsive (positive). The effective $\Re t_{N\bar{N}}$ is density dependent and has a complicated structure. At the nuclear surface it reflects a long attractive tail of the pion exchange forces, at distances around the nuclear radius it may turn to repulsion due to repulsive scattering lengths, and it is rather uncertain at the nuclear matter densities. On the other hand, the phenomenological best fit $\Im t_{N\bar{N}}$ represents cumulative effect of the S and P wave absorptive amplitudes and can be well understood in terms of the free $\Im t_{N\bar{N}}$. Theoretical optical potentials are more complicated than formula (1), but do not reproduce the data as accurately as the latter with the best fit parameters.

The level widths reflect all modes of nuclear absorption. The initial stage of this process, an elementary $N\bar{N}$ annihilation, generates ≈ 2 GeV energy that turns mostly into kinetic energy of the final state mesons. These mesons excite residual nuclei by inelastic processes. To calculate the widths one sums over unobserved nuclear excited states. The large energy release allows a closure over these states and the effective $\Im t^{N\bar{N}}$ is close to the absorptive part of the free $\Im t^{N\bar{N}}$. This is not true when final nuclear states are limited by the measurements. Thus, the radiochemical detection allows only cold nuclei i.e. nuclei either in the ground states or excited less than the neutron separation threshold, [3]. The effect of this limitation is discussed in the next section.

3 Nuclear $N\bar{N}$ Annihilation and Final State Interactions

The aim of this section is to calculate the rate of nuclear \bar{p} annihilations that lead to cold final nuclei. This is done in few steps:

- 1) An amplitude for the $N\bar{N}$ annihilation into mesons $t_{N\bar{N} \rightarrow M}$ is assumed and introduced into the nuclear transition amplitude in the impulse approximation.
- 2) The emission probabilities are calculated and summed over mesonic and nuclear final states. For an isolated $N\bar{N}$ annihilation this procedure would produce the absorptive cross section and via unitarity condition the absorptive amplitude $\Im t_{N\bar{N}}$. For nuclear captures leading to cold nuclei we limit the summation over final states to the states of elastic meson nucleus scattering. This limited summation generates the $\Im t_{N\bar{N}}$ again, but now it is folded over nuclear final state interaction factors, $P_{\text{miss}}(\vec{R})$, which describe the probability that the annihilation mesons born at point \vec{R} miss the residual nucleus.
- 3) Let a nucleon N occupy a single particle level α with a wave function $\varphi_\alpha(\vec{X})$. Then, the $\bar{p}N$ annihilation process limited by P_{miss} leads to a single hole final nuclear state. The experimental condition allows only those initial levels

α that end in cold final nuclei. A factor $P_{\text{dh}}(\vec{X}) = \sum_{\alpha}^{ltd} \varphi_{\alpha}^2 / \sum_{\alpha} \varphi_{\alpha}^2$ accounts for this condition.

4) The finite range effects are described by separable potentials as done in [11].

The result for a partial width corresponding to a cold capture on a nucleon $s =$ (proton or neutron) is now

$$\Gamma_s(\text{cold}) = 4 \frac{\pi}{\mu_{N\bar{N}}} \Im t_{N\bar{N}}^s \int | \Psi_{\bar{N}}(\vec{Y}) |^2 v(\vec{Y} - \vec{X}) \rho_s(\vec{X}) P_{\text{dh}}(\vec{X}) P_{\text{miss}}(\vec{R}) \quad (4)$$

where $t_{N\bar{N}}^s$ is an effective length and \vec{R} is the birthplace of the mesons. The assumption, justified later, is that all the mesons are emitted from the central point of the annihilation region $\vec{R} = \frac{\vec{X} + \vec{Y}}{2}$.

Eq.(4) is the result, now we explain briefly the final state interactions that determine P_{miss} and in the next section we turn to calculations of the nuclear densities.

The spectrum of mesons consists essentially of pions correlated in a sizable fraction into ρ and ω . These heavy mesons propagate some 1 fm and then turn into pions. The pion multiplicities range from 2 to 8 with an average 4–5 and an average momentum as large as 400 MeV. Nuclear interactions of these pions may be absorptive, inelastic or elastic. All the absorptive and almost all the inelastic processes would not leave the residual nuclei in cold states and so the production rate for the latter is given essentially by the elastic scattering. This allows an optical potential description. In addition, in the bulk of phase space the pions are fast enough to allow also an eikonal description. Following this, the wave function for each pion is taken in the form

$$\bar{\psi}^{(-)}(\vec{p}\vec{\xi}) = \exp(i\vec{p}\vec{\xi} - iS(\vec{p}, \vec{\xi})) \quad (5)$$

where \vec{p} is a momentum, $\vec{\xi}$ is a coordinate and S is expressed in terms of the pion-nucleus optical potential

$$S(\vec{p}, \vec{\xi}) = \int_0^{\infty} ds (\sqrt{(p^2 - U^{\text{opt}}(\vec{\xi} + \hat{\vec{p}}s))} - p) \quad (6)$$

The S is calculated by integrating the local momentum over the straight line trajectory. Due to nuclear excitations and pion absorptions this wave is damped with a rate described by $\Im S$. The latter is generated by absorptive part of the pionic optical potential $\Im U^{\text{opt}}$. This damping follows the whole path but the main effect comes from regions of large nuclear densities and not the region around the birth place $\vec{\xi}$. We assume that all functions $S(\vec{p}, \vec{\xi})$ are related to the central point of annihilation \vec{R} that is the $N\bar{N}$ CM coordinate. With the mesonic wave functions (5) the dependence on the total momentum of mesons \vec{P} factorizes approximately to a plane wave form. One consequence is that the $N\bar{N}$ CM "conservation" $\delta(\vec{R} - \vec{R}')$ arises in the transition probabilities integrated over

final momenta. Now, the final state pion interaction factors may be collected into a probability distribution

$$P_{\text{miss}}(\vec{R}) = \langle \prod | \exp(-S(\vec{p}_i, \vec{R})) |^2 \rangle \quad (7)$$

It is a product of the eikonal factors averaged over the number and phase space of final pions with some allowance for an unknown momentum dependence generated by $t_{N\bar{N} \rightarrow M}$.

The calculations of P_{miss} are performed in a Monte Carlo procedure. The optical potential for pions must cover wide momentum range from the threshold up to 0.9 GeV but the phase space favours a region just above Δ resonance. This potential is related to the pion nucleon forward scattering amplitudes and in this way to the pion nucleon cross sections. That method is established around the Δ [13]. Here, it is extended to higher N_{11}^* , N_{13}^* resonances which are described by Breit-Wigner amplitudes. The two nucleon absorption mode is taken in a phenomenological form [14]. Performing these calculations one finds that: high energy expansion of the square root in Eq.(6) is satisfactory, higher resonances cannot be neglected and the black sphere limit is a good approximation in dense regions. The result is close to a pure geometrical estimate that relates $P_{\text{miss}}(\vec{R})$ to the solid angle of the nucleus viewed from the point \vec{R} [9]. In the surface region of interest the P_{miss} is a linear function of the radius. It is very fortunate, it makes this calculation fairly independent on the size of the $N\bar{N}$ annihilation region and on the uncertain range of the heavy meson propagation.

Examples of P_{miss} , P_{dh} and the density A for cold absorption generated by Eq.(4) are given in Fig.1. The latter is seen to be more peripheral than the total absorption density W . The uncertainty due to the $N\bar{N}$ force range is rather small, being moderated by effects of the strong absorption. The uncertainty of the initial atomic state is shown in Table 1. The ratio of cold to total capture rates Γ^c/Γ^t raises quickly with the increasing angular momentum. The experimental results, given in Table 2, indicate that a significant contribution of high l states is unlikely. On the other hand, some participation of lower l states is possible. However, due to the atomic cascade properties, that seems to be unlikely. A definitive answer requires experimental and theoretical studies which are being undertaken, [6].

The absorption widths are given by superpositions of high moments of the nuclear density distributions. We find the $2l - 2$ moment as the dominant one for the total widths and the $2l$ moment to dominate the cold capture width. The "neutron halo" is thus understood as a ratio of these high moments of neutron and proton density distributions. The "neutron skin" is related the m.sq. radius or other low moments.

Table 1: Column 2 contains main quantum number n for the lower and upper circular states. The weights give probabilities for nuclear capture calculated under the assumption that the circular atomic state $n = n_{\text{upper}} + 1$ is fully occupied. The absorption widths: total Γ^t and cold Γ^c are calculated with the AD model, $R_{np} = .63$.

ELEMENT	n	weight	Γ^c/Γ^t	Γ_n/Γ_p
^{58}Ni	4	0	.095	.69
	5	.16	.097	.69
	6	.83	.11	.70
	7	.01	.15	.71
	8	0	.22	.71
^{90}Zr	6	.24	.106	4.67
	7	.72	.128	5.30
^{154}Sm	7	.01	.087	3.65
	8	.75	.099	3.98
^{238}U	9	.29	.106	6.55
	10	.71	.138	8.24

4 Nuclear Densities

As the simplest estimate we use an asymptotic density (AD) model. It follows the Bethe-Siemens approach [12] although the larger input includes: charge density distribution, neutron and proton separation energies and difference of the rms radii of proton and neutron density distributions. At central densities a Fermi gas of protons and neutrons is assumed. The Fermi momenta are determined by the densities and Fermi energies are fixed by the separation energies. This gives depth of the potential well which in the surface region is extrapolated down in the Woods-Saxon form. The densities are given by the exponential damping of the nucleon wave functions due to the potential barriers. For protons a Coulomb barrier is added and potential parameters (c, t) are fitted to reproduce the experimental charge density down to 5 percent of the central density. For neutrons the same t is used but c is chosen to obtain the rms radius equal (or larger by 0.05 fm in the heaviest nuclei) to the proton density rms radius. This model is expected to generate average level densities, it misses shell effects and correlations.

A second model used to determine neutron and proton densities is the Hartree-Fock (HF) and the Hartree-Fock-Bogolyubov (HFB) scheme with the effective two-body Skyrme-type interaction. Our aim in using HF and HFB methods to find nucleon densities at the extreme tails of the nuclear matter

distribution (at distances of 8–15 fm from the center) is rather unusual. The necessary practical condition is the use of a HF code not restricting the asymptotic form of s.p. wave functions. This excludes e.g. all codes using the harmonic oscillator basis. In the present work we have applied the code solving HF equations on the spatial mesh, in which all fields and densities are expressed in the coordinate representation.

The HF method disregards completely pairing correlations. To account for them we used the HFB theory [16,17] which unifies the self-consistent description of nuclear orbitals, characteristic of HF method, and the mean field treatment of residual pairing interaction into a single variational theory. The effective force is the ten-parameter Skyrme SkP interaction described in ref [18]. It has a virtue that the pairing matrix elements are determined by the force itself, contrary to other Skyrme-type interactions which define only the particle-hole channel. The paired HFB ground-state has not the BCS form so there is no simple pairing gap parameter although a kind of average gap can be defined as the pairing potential average over occupied states.

The most severe restriction of the presented results is the imposed spherical symmetry, both in the HF and HFB codes. It allows enormous simplification of solutions, in particular the HFB equation takes the form of two coupled differential equations in the radial variable for each value of s.p. angular momentum.

The density matrix is obtained by summing contributions from the lowest s.p. orbits. The degeneracy of the spherical subshells is handled by taking contribution of the last orbit in the filling approximation, i.e., an appropriate occupation probability smaller than one is, if necessary, associated with this orbit.

Some results are collected in Table 2. To find Γ_n/Γ_p a ratio of $\bar{p}n$ and $\bar{p}p$ absorptive amplitudes R_{np} is needed. One number $R_{np} = .63$ follows from mesonic studies in ^{12}C [4]. It depends on uncertain final charge exchange processes and we use the deuteron value $R_{np} = .82$ [15]. The latter coincides with a good fit to Γ_n/Γ_p in ^{58}Ni .

Our conclusions are:

- 1) The AD model overestimates the neutron haloes. The latter are not given by the binding energies and Coulomb barriers alone. The shell effects (angular momentum) are essential, correlations of HFB type have rather small effect. These conclusions are similar to the results of subcoulomb neutron pickup studies [19].
- 2) Even at these nuclear peripheries at least 2-3 nucleon orbitals are involved in the capture.
- 3) There are two anomalous cases: Yb and Te. The anomalies are apparently related to a strong E2 mixing in those atoms.
- 4) An interesting case of proton halo is seen in ^{144}Sm . It is not understood yet.

Table 2: Experimental and calculated results for Γ^c/Γ^t and Γ_n/Γ_p . Calculations are averaged over few atomic orbitals weighted as in Table 1, with $R_{np} = .82$.

	Γ^c/Γ^t	Γ_n/Γ_p	Γ^c/Γ^t	Γ_n/Γ_p	Γ^c/Γ^t	Γ_n/Γ_p
	Exp. [3]		Asympt.		HF	
^{58}Ni	.098(8)	0.9(1)	.11	.90	.110	.785
^{90}Zr	.161(22)	2.6(3)	.12	4.9	.125	2.54
^{96}Ru	.113(17)	0.8(3)	.10	1.7	.099	.944
^{130}Te	.184(36)	4.1(1)	.12	2.6	.124	3.14
^{144}Sm	.117(20)	$\leq .4$.09	1.9	.094	1.38
^{154}Sm	.121(20)	2.0(3)	.10	5.1	.110	3.34
^{176}Yb	.241(40)	8.1(7)	.12	4.8	.111	3.23
^{232}Th	.095(14)	5.4(8)	.12	7.6	.087	3.80
^{238}U	.114(9)	6.0(8)	.13	10	.092	4.09

5) The antiprotonic study of nuclear surface is a promising method, despite some uncertainties.

The authors acknowledge support by KBN Grants 2 P302 010 07 and Pb2 0956 91 01

References

- [1] D.H. Wilkinson: Phil. Mag. **4**, 215 (1959)
- [2] C.J. Batty: Rep. Prog. Phys. **52**, 1165 (1989); C.J. Batty et al.: Adv. Nucl. Phys. **19**, 1 (1989)
- [3] J. Jastrzębski et al.: Nucl. Phys. **A558**, 405c (1993); P. Lubiński et al.: Phys. Rev. Lett **73**, 3199 (1994)
- [4] W.M. Bugg et al.: Phys. Rev. Lett. **31**, 475 (1973); M. Leon and R. Seki: Phys. Lett. **48B**, 173 (1974)
- [5] D.H. Davis et al.: Nucl. Phys. **B1**, 434 (1967); E.H.S. Burhop: Nucl. Phys. **B1**, 438 (1967); Nucl. Phys. **B44**, 445 (1972)
- [6] The CERN Proposal, Experiment PS 209; S.Wycech et al.: to be published
- [7] Th. Kohler et al.: Phys. Lett. **B176**, 327 (1986); D. Rohmann et al.: Z. Phys. **A325**, 261 (1986); C.J. Batty: Nucl. Phys. **A372**, 433 (1981)

- [8] C.J. Batty: Phys. Lett. **B189**, 393 (1987); E. Friedman and J. Lichtenstadt: Nucl. Phys. **A455**, 573 (1986)
- [9] J. Cugnon and J. Vandermeulen: Ann. Phys. (Paris) **14**, 49 (1989)
- [10] T. Suzuki and H. Narumi: Nucl. Phys. **A426**, 413 (1984); S. Adachi and H.V. von Geramb: Acta Phys. Aust. **XXXVII** 627 (1985); Nucl. Phys. **A470**, 461 (1987); O.Dumbrajs et al.: Nucl. Phys. **A457**, 491 (1986)
- [11] A.M. Green and S. Wycech: Nucl. Phys. **A467**, 744 (1987); Nucl. Phys. **A377**, 441 (1982)
- [12] H. Bethe and Ph. Siemens: Nucl. Phys. **B21**, 587 (1970)
- [13] L.C. Liu and C.M. Shakin: Phys. Lett. **B78**, 389 (1978)
- [14] J.N. Ginocchio: Phys. Rev. **C17**, 195 (1978)
- [15] R. Bizzari et.al.: Nuovo Cim. **22A**, 225 (1974)
- [16] N.N. Bogolyubov: JETP (Sov. Phys.) **7**, 41 (1958); Sov. Phys. Usp. **2**, 236 (1959); Usp. Fiz. Nauk **67**, 549 (1959)
- [17] P. Ring and P. Schuck: *The Nuclear Many-body Problem*. New York: Springer 1980
- [18] J. Dobaczewski, H. Flocard and J. Treiner: Nucl. Phys. **A422**, 103 (1984)
- [19] H.J. Körner and J.P. Schiffer: Phys. Rev. Lett. **27**, 1457 (1971)